Cell Communication and Signaling

RESEARCH

Open Access

CXXC5 function blockade promotes diabetic wound healing through stimulating fibroblast and vascular endothelial cell activation

Yutong Chen[1*†], Xiaofeng Ding[2†], Zhouji Ma[3,4†], Shuai Shao[1†], Heyan Huang[5], Yumeng Huang[6], Beizhi Wang[7], Hao Zhang[1] and Qian Tan[1,8*]

Abstract

Background Extracellular matrix (ECM) and angiogenesis are critical controls of wound regeneration, and their dysfunction delays diabetes recovery. CXXC5 belongs to the CXXC protein family that can regulate the function of human dermal fibroblasts (HDFs) and human umbilical vein endothelial cells (HUVECs); However, awareness of its functional role remains limited.

Methods Mice were divided into control (CON), diabetic (DM), diabetic + KY19382 (DM + KY19382), and diabetic + vehicle (DM + Vehicle) groups. HDFs and HUVECs were stimulated under different CXXC5 conditions and mice were treated with KY19382, followed by the application of assays including Western blotting (WB), immunofluorescence (IF) and quantitative reverse transcription-PCR (qRT-PCR) to assess wound healing and molecular signaling.

Results Mice in DM had fewer blood vessels, a slower wound healing rate, and more disrupted collagen than CON. Application of KY19382 improved these conditions, which promoted fibroblast activation and vascularization in high glucose environments and DM. Mechanistically, blocking CXXC5 promotes Wnt/β-catenin-mediated stabilization by reducing the binding of the deterrent factor CTBP1 to β-catenin, which induces dermal fibroblast activation and facilitates HUVECs tube formation and migration via VEGFA/VEGFR2 and NFκB signaling pathways. KY19382 promotes HUVECs activation by blocking CTBP1 transcription to activate the NFκB signaling pathway, thus wound re-vascularization.

Conclusion CXXC5 is an essential regulatory factor of wound healing and a prospective therapeutic target for treating chronic wound damage in diabetes.

Keywords CXXC5, Fibroblast, Angiogenesis, Wound healing, Diabetes

†Yutong Chen, Xiaofeng Ding, Zhouji Ma and Shuai Shao contributed equally to this work.

*Correspondence:
Yutong Chen
985881572@qq.com
Qian Tan
smmutanqian@sina.com

Full list of author information is available at the end of the article

Introduction

Diabetes is one of the prevalent chronic intractable diseases characterized prominently by hyperglycemia, seriously jeopardizing human physical and mental health worldwide [1, 2]. Chronic diabetic foot ulceration (DFU) is one of the most devastating complications of diabetes [3], with a global prevalence of approximately 6.3% [4]. DFU have a lifetime prevalence of 19–34% [5]. Nearly 20% of moderate and severe infected DFU eventually lead to amputation [5, 6], with a 5-year mortality rate approaching 50% [7]. Currently, the treatment of diabetic wounds remains limited, consisting mainly of glycemic stabilization and removal of localized necrotic tissue up to amputation, which disappointingly fails to lessen the burden of life of patients [8]. Therefore, further investigation of the underlying pathological mechanisms of impaired wound repair is warranted to develop effective targeted drugs.

A hyperglycemic environment impedes the conventional wound repair pathway, and diabetic wounds are characterized by a prolonged inflammatory phase accompanied by inhibition of angiogenesis and extracellular matrix (ECM) synthesis [9]. Major fibrous protein that builds the ECM in the dermis is collagen, composed of collagen types I and III, and form a cross-linked network that provides a platform for cell migration [10]. While, proliferation and migration of endothelial cells and fibroblasts into the wound area are key factors in ECM deposition and neovascularization [2, 11]. Fibroblasts are abundant in connective tissue and accelerate wound repair by releasing growth factors, producing the ECM in the dermis, and enhancing wound closure [12]. In addition, fibroblasts secrete several regulatory mediators, including vascular endothelial growth factor (VEGF), which promotes endothelial cell proliferation, migration and lumen formation [13, 14]. VEGF is classified from type A to type F, in which VEGFA is predominant and regulates angiogenesis at different stages. VEGFA can increase vascular permeability in the inflammatory stage, stimulate endothelial cell proliferation in the proliferation stage, and induce lumen formation in the remodeling stage, which has become one of the essential factors in regulating angiogenesis [15]. It is expected that the exploration of such inducers of ECM and vascular regeneration will have therapeutic relevance for the acceleration of diabetic skin wound regeneration.

The Wnt/β-catenin signaling pathway is of great importance in cutaneous dermal fibrotic, ECM deposition and wound healing [16]. It is characterized by raised β-catenin expression and nuclear accumulation during the proliferative phase of skin repair. Activating the Wnt/β-catenin signaling pathway has been demonstrated to induce myofibroblast differentiation and dermal fibrosis, thus facilitating the process of skin healing [17].

The NFκB signaling pathway has received increasing attention as an essential regulatory pathway for angiogenesis and cell proliferation [18–20]. A major trigger for activation of the NFκB pathway is ectopic nuclear translocation of nuclear factor-κB (NFκB), a universal transcription factor consisting of p50, p65 and IκBa subunits [18]. When the NFκB signaling pathway is activated, phosphorylation of IκBa in the cytoplasm dissociates the dimer, which allows NFκB to be exposed and incorporated into the nucleus to form a more stable p-NFκB, facilitating the transcription of related genes [21]. In glioblastoma models, the inhibition of NFκB-reduced the pro-angiogenic factor VEGF [22]. Similarly, NFκB and VEGF-targeting agents can produce anti-angiogenic and impaired wound healing side effects in the clinic [23]. Consequently, numerous research studies have demonstrated that elevated levels of NFκB activity can facilitate angiogenesis [24]. Therefore, activation of Wnt/β-catenin signaling pathway and NFκB signaling pathway may be a therapeutic target for diabetic wound healing.

CXXC5 is a member of the CXXC family of zinc finger proteins [25]. It is a negative regulator of the Wnt/β-catenin signaling pathway. As a transcriptional activator, CXXC5 stimulates Flk-1 transcription and induces embryonic endothelial differentiation, migration and angiogenesis in mouse embryonic stem cells (mESCs) [26]. In addition, cytoplasmic accumulation of CXXC5 and negative regulation of Wnt/β-catenin signaling pathway have been observed in a variety of diseases such as osteoporosis, alopecia, and metabolic disorders, which impedes the regeneration of damaged tissues [27–29]. CXXC5 has been shown to function by interacting with upstream Dishevelled (Dvl) to block activation of the Wnt/β-catenin signaling pathway [17, 25]. PTD-DBM peptides and small molecule mimics of PTD-DBM peptides, such as KY19382 and KY19334, have been shown to interfere with CXXC5-Dvl interactions to activate Wnt/β-catenin signaling pathway [16, 30–32]. The efficacy of KY19382 has been further confirmed in disease models such as improved wound healing, baldness and metabolic disorders [28, 29, 32].

However, the specific molecular mechanisms by which CXXC5 negatively modulates the Wnt/β-catenin signaling pathway and modulates ECM deposition and endothelial differentiation have not been clearly elucidated in most in vitro cell culture studies. In this research, the function of CXXC5 on wound repair in streptozotocin-induced diabetic mice (DM) was evaluated by assessing angiogenesis, collagen deposition, and re-epithelialization. In addition, we found that blockade of CXXC5 function activated the Wnt/β-catenin, VEGFA/VEGFR2 and NFκB signaling pathways during skin repair, with the involvement of paracrine effects of fibroblasts on endothelial cells and the transcriptional regulator CTBP1.

Collectively, our findings suggest that blockade of CXXC5 function might be a possible therapy for the treatment of delayed wound healing in diabetes.

Methods

Cell lines

HUVECs and HDFs were sourced from the Shanghai Institutes for Biological Sciences, Chinese Academy of Sciences. HDFs were incubated in Dulbecco's modified Eagle's medium (DMEM), supplemented with 40 mM D-glucose, 1% Penicillin-Streptomycin-Amphotericin B Solution (Keygen, China), and 10% fetal bovine serum (FBS). HUVECs were cultured in the medium used for endothelial cells (ECM; ScienCell, USA) containing 40 mM D-glucose and 10% FBS. Standard conditions were provided for all cells (37 °C, 5% CO_2).

Cell transfection

CXXC5 gene-targeting shRNA lentivirus carrying the U6-shRNA-gcGFP-puro plasmid or the control non-specific shRNA lentivirus (GeneChem, Shanghai, China) were transfected into HUVECs and HDFs. After 8 h of transfection, the medium was altered to a fresh medium. 1 μg/ml of puromycin was used for 2 days to construct stable knockout cells and then cultured in DMEM added with puromycin (0.5 μg/ml).

Immunofluorescence assay

Cells were seeded in 24-well plates (3524, Corning, USA) overnight. Phosphate-buffered saline (PBS, 10mM, pH = 7.4, Keygen, China) was rapidly added to rinse the cultured cells twice and later fixed in 4% paraformaldehyde (NCM Biotech, China) at room temperature for 15 min. After rinsing three times with PBS for 3 min, the cells were osmolised with 0.2% Triton X-100 for 10 min (Beyotime, China). After blocking in solution (Beyotime, China) for 1 h under normal temperature, the cells were processed with primary antibodies at 4 °C overnight (Anti-CXXC5, 1:50, Santa Cruz Biotechnology, USA; Phospho-NFκB, 1:800, CST, USA) and secondary antibodies in the dark for 1 h. DAPI (Sigma-Aldrich, USA) was stained for 10 min under normal temperature and rinsed with PBS. Images were captured using a DMi8 Inverted fluorescence microscope (Leica Microsystems, Germany).

Western blot analysis

Cells in 6-well plates (3516, Corning, USA) were collected and lysed by adding RIPA buffer added with 1% protease inhibitors (PMSF) and phosphatase inhibitors (Solarbio, China). Subsequently, the lysate was transferred to an EP tube and subjected to 30 min of centrifugation at 12,000 rpm, 4 °C. The amount of protein in each sample was quantified utilizing the BCA kit (Beyotime, China). Target proteins were isolated by SDS-polyacrylamide gel electrophoresis and then migrated to polyvinylidene difluoride (PVDF) membranes (Millipore, IPFL00010, USA) at a low temperature. Membranes were blotted with primary antibodies overnight at 4 °C on a slow shaker after blocking with 5% bovine serum albumin (BSA) for 1 h at room temperature. Primary antibodies are as follows: Anti-CXXC5 (1:2500, #822172, ZEN-BIOSCIENCE, China), Anti-β-catenin (1:5000, ab32572, Abcam, USA), Anti-COL1a1 (1:1000, #72026, CST, USA), Anti-α-SMA (1:1000, ab124964, Abcam, USA), Anti-CD31 (1:1000, A19014, ABclone, China), Anti-CTBP1 (1:1000, ab129181, Abcam, USA), Anti-VEGFR2 (1:1000, ab134191, Abcam, USA), Anti-VEGFA (1:1000, ab214424, Abcam, USA), Anti-p-IκBα (1:5000, ab133462, Abcam, USA), Anti-IκBα (1:5000, ab32518, Abcam, USA), Anti-p-NFκB (1:1000, #3303, CST, USA), Anti-NFκB (1:1000, #8242, CST, USA), Anti-PCNA (1:5000, ab92552, Abcam, USA), Anti-TCF1/TCF7 (1:1000, #2203, CST, USA), Anti-p-IKKα(Ser176)/IKKβ(Ser177) (1:1000, #2078, CST, USA), Anti-p-IKKα/β(Ser176/180) (1:1000, #2697, CST, USA), Anti-IKKα (1:1000, #61294, CST, USA), Anti-β-actin (1:4000, 81115-1-RR, Proteintech, USA). Membranes were rinsed three times with TBST and reacted with an anti-rabbit IgG Horseradish enzyme labeled secondary antibody (1:30000, ZB-2301, Zhongshan Jinqiao, China) under normal temperature for 1 h. Finally, an enhanced ECL reagent (Vazyme, China) and the Tanon Chemi-Image system were used to image the protein bands.

RNA isolation and quantitative reverse transcription-PCR (qRT-PCR)

Total RNA was purified from cell lysates and cryogenically ground tissue powder using TRIzol reagent (R410, Vazyme, China), followed by cDNA preparation using a reverse transcription kit (R333, Vazyme, China) in accordance with the manufacturer's instructions. A SYBR qPCR kit (Q712, Vazyme, China) was used to perform quantitative PCR in 96-well plates (402001, NEST, China) under the following settings: pre-denaturation at 95 °C for 30 s, followed by 40 cycles at 95 °C for 10 s, and a reaction temperature of 60 °C for 30 s. The following primer sets were employed: CXXC5, forword 5′-CAAG AAGAAGCGGAAACGCTGC-3′ and reverse 5′-TCTCC AGAGCAGCGGAAGGCTT-3′. GAPDH, forword 5′-A CCACAGTCCATGCCATCAC-3′ and reverse 5′-TCCA CCACCCTGTTGCTGTA-3. GAPDH was employed as control for the normalization of target mRNA levels.

Tube formation assay

Matrigel (Corning, USA) was melted at 4°C overnight for gel preparation. A 50 μl of Matrigel volume was added to a 96-well plate (3596, Corning, USA) using pre-cooled

pipette tips and maintained for 40 min at 37 °C. HUVECs were seeded at a density of 3×10^4 and cultured with different media. Tube formation was observed 4 h later under a microscope.

Cell counting kit-8 (CCK8) assay

Logarithmic growth stage cells were harvested, resuspended by trypsinization, and plated in 96-well plates (3596, Corning, USA) (2000 cells/well). After adding 10 µl of CCK8 solution (APExBIO, USA) to each well, the cells were incubated for 2 h. Optical density (OD) was read at 450 nm using a microplate reader. The OD value was used to detect the cell proliferation ability of the different groups at different times.

Scratch wound assay

For the scratch wound tests, the cells were first spread in 6-well plates (3516, Corning, USA) until completely covered. After the monolayer was scraped vertically using a 200ul tip, the isolated cells were washed with PBS. The cultured cells were then replenished with basal medium. Cellular wounds were captured on days 0 and 1.

Transwell assay

The target migrating cells were seeded in the upper chamber of the Transwell, and 10% FBS medium was introduced to the bottom compartment (Corning, USA). Subsequently, the cells were placed at 37 °C for 24 h. Cells were maintained in 4% paraformaldehyde for 20 min, immersed in crystal violet (Sigma-Aldrich, USA) for a further 20 min under normal temperature, washed 3 times with PBS, and visualized using an inverted microscope (Olympus, Japan). Three random microscopic areas (magnified 100x) were counted.

mRNA library construction sequencing

TRIzol reagent was added to separate total RNA from HDFs (Invitrogen, Carlsbad, CA, USA), and the resulting material was purified using RNase-free DNase I (Takara, Kusatsu, Japan). The integrity of the RNA was assessed through 1% agarose gel electrophoresis, which was employed to monitor any potential degradation or contamination. RNA quantification was assessed employing an Agilent 2100 Bioanalyzer (Agilent Technologies, CA, USA), and the quality and intactness of the RNA were evaluated using a NanoDrop spectrophotometer (Thermo Scientific, DE, USA). Sequencing libraries were prepared according to the producer's guidelines with the NEBNext® Ultra™ RNA Library Prep Kit for Illumina® (NEB, USA). To assign sequences to each sample, index codes were then incorporated. In essence, mRNA was isolated from the overall RNA sample by employing poly T-tagged magnetic beads. The purification of the PCR products was conducted on the AMPure XP system, and the qualitative assessment of the library was performed within the Agilent Bioanalyzer 2100 system. The library was prepared on an Illumina Novaseq 6000 platform on behalf of Beijing Allwegene Technology Company Limited (Beijing, China), resulting in paired-end reads of 150 bp.

RNA-seq data analysis

Raws (reads) were initially processed using proprietary Perl scripts to generate clean (FASTQ-formatted) data. This involved the removal of adapter sequences, low-quality sequences, and poly-N sequences from the raw data. The sorting and removal of duplicated reads, along with the merging of the beam alignment results, were conducted using sam-tools v0.1.18 and Picard-tools v1.41. HTSeq v 0.5.4 p3 was employed to enumerate the number of reads that aligned to each gene. Differential expression of both samples was conducted utilizing the DEGseq (2010) R package. The statistically significant enrichment of the differentiation genes in the pathways of the Kyoto Encyclopedia of Genes and Genomes (KEGG) was checked with the KOBAS software. The sequences of the differentially expressed genes (DEGs) were undergone BLAST (blastx) analyses against the genome of a related species, to identify protein-protein interactions that could be taken from the STRING database (http://string-db.org/).

Cytoplasmic and nuclear fractionation

The HDFs were rinsed once with PBS and retrieved using cell scrapers. A nuclear and Cytoplasmic Extraction Kit (R0050, Solarbo, China) was performed to isolate nuclear and cytoplasmic proteins. After protein fractionation, WB was applied to analyze the level of β-catenin protein in the cytoplasm and nuclear. Lamin A + C (1:1000, ab315838, Abcam, USA) and β-actin (1:4000, 81115-1-RR, Proteintech, USA) were assessed as nuclear and cytoplasmic markers, respectively.

Immunoprecipitation (IP)

HDFs and HUVECs were lysed with inhibitor-containing lysate, and the product (500 µg protein) with protein A + G magnetic beads (P2179, Beyotime, China) and appropriate anti-β-catenin antibody (1:30, ab32572, Abcam, USA), anti-TCF1/TCF7 antibody (1:50, #2203, CST, USA), Anti-VEGFR2 (1:20, ab134191, Abcam, USA), Anti-IκBα (1:20, ab32518, Abcam, USA) and Anti-NFκB (1:100, #8242, CST, USA) was rotated overnight at 4 °C in accordance with the manufacturer's instructions. Membranes were then reacted with secondary antibody (1:2000, A25022, Abbkine, China) under normal temperature for 1 h. After magnetic separation, the products were subjected to WB analysis to evaluate potential protein-protein interactions.

Establishment of diabetic mice model

Single Male C57BL/6 mice (6–8 weeks, initial weight about 20 g) were acquired from the Laboratory Animal Center of Nanjing University. In strict accordance with the SPF standard, 6 mice were randomly assigned per cage and adaptively fed for 1 week at the Animal Center of Nanjing Drum Tower Hospital, with 12 h alternating daylight and adequate food and water. The proposed animal experiment has been authorized by the Medical School for Animal Use and Care Committee of Nanjing Drum Tower (Ethics Approval Number: DWSY-22083209) in adherence to ARRIVE guidelines. Mice were randomly (simple randomization) divided into CON, DM, DM + Vehicle, and DM + KY19382 groups ($n = 6$). After an overnight fast, C57 mice were induced by intraperitoneal injection of streptozotocin (pH = 4.0, dissolved in 0.1 mM citrate buffer, 50 mg/kg) for 5 continuous days. The model was successfully established when the blood glucose level of the mice remained above 16.7 mM for 4 consecutive weeks and a full-thickness incision of 1 cm in diameter was made on the dorsal side of the mice. 2 and 3 mice in the diabetic group died due to hyperglycemia and hypothermia after anesthesia, respectively, while no deaths occurred in CON. A silicone stent with a thickness of 0.6 mm was sutured around the wound to prevent skin contraction, and the dressing was changed daily. DM were intradermally injected with 100 μl KY19382 (HY-131447, MCE, USA) (1mM) [33] on days 0, 2, 4, 6, 8, and 10, while CON were injected with the same volume of Vehicle. The alterations in the wound area of each group were documented photographically and analyzed using the ImageJ software. Wound margin tissue was detected using hematoxylin-eosin (HE) staining, WB, Masson's trichrome (MT) staining, RT-qPCR, and IF.

Hematoxylin-eosin (HE) and Masson's trichrome (MT) staining

Once the sections were laid flat, fixed, dehydrated, and paraffin-embedded, a thickness of 5 μm was achieved. The sections were deparaffinized by means of xylene, followed by gradient alcohol hydration, and then stained with HE and MT.

Immunofluorescence (IF) staining

To examine the levels of CXXC5 and β-catenin, the sections above were treated with anti-CXXC5 (1:50, Santa Cruz Biotechnology, USA), anti-β-catenin (1:200, ab32572, Abcam, USA), and anti-Keratin 14 (1:800, 10143-1-AP, Proteintech, USA) at 4 °C overnight, then further stained with fluorescent secondary antibody (1:1000, ab150077, Abcam, USA or 1:1000, ab150116, Abcam, USA) at room temperature for 1 h. After fixing with DAPI (Sigma-Aldrich, USA), the sections were imaged and documented within a TCS SP8 laser confocal microscope (Leica Microsystems, Germany).

Immunohistochemistry (IHC) staining

Paraffin tissue Sect. (5 μm thickness) were deparaffinized, hydrated, antigenically repaired, and exposed to PBS consisting of 0.2% Triton X-100 for 15 min, after which they were cooled to normal temperature. After blockade with 5% BSA, the sections were reacted with anti-CXXC5 (1:50, Santa Cruz Biotechnology, USA), Anti-VEGFA (1:100, ab52917, Abcam, USA), Anti-CD31 (1:600, A19014, ABclone, China) and Anti-p-GSK3β (1:50, ab68476, Abcam, USA), and left at 4 °C overnight. After rewarming, the reaction was repeated with goat anti-rabbit HRP-conjugated secondary antibody (1:20000, ab205718, Abcam, USA) for 1 h at normal temperature. 3, 3-Diaminobenzidine (DAB, 1:20, Sigma, USA) was used for development, and hematoxylin (Solarbio, China) was supplement to stain the nuclear for 1 min. The sections were capped with neutral gum (Solarbio, China). The results were evaluated via a TCS SP8 laser confocal microscope (Leica Microsystems).

Statistical analysis

All data were given as mean ± standard deviation (SD) and statistically analyzed using GraphPad Prism software. Statistical analysis was conducted using Student's t-test or one-way analysis of variance (ANOVA), and two-way ANOVA. Normality was assessed with the Shapiro–Wilk test. The unpaired Student's t-test was used for normally distributed data to analyze comparisons between the two groups; otherwise, the Mann–Whitney nonparametric test was used. Multiple pairwise comparisons have been adjusted for significance by the Bonferroni correction. Statistically meaningful results were expressed as ($^{*}P < 0.05$; $^{**}P < 0.01$; $^{***}P < 0.001$). Results were regarded as non-significant (ns) when the p-value was over 0.05.

Results

Diabetic mice display chronic wound healing

To understand the function of CXXC5 in skin regeneration in a diabetic mouse model, we generated 10 mm diameter injuries on the backside of the mice. Compared with the scars in DM, the wound size in CON was significantly reduced at days 3 ($P < 0.05$), 7 ($P < 0.05$), 10 ($P < 0.01$), and 14 ($P < 0.05$) (Fig. 1A). MT staining at day 10 showed a markedly diminished level of collagen deposition in the DM in comparison to the CON. (Fig. 1B). HE staining assay also demonstrated that the gap between wound margins was reduced in DM (Fig. 1D). Concentrations of β-catenin and CXXC5 during the repair progress in mouse wound tissue samples were evaluated by using IHC (Fig. 1C), WB (Fig. 1E), qRT-PCR (Fig. 1F), and IF (Fig. 1G). The results indicated elevated CXXC5

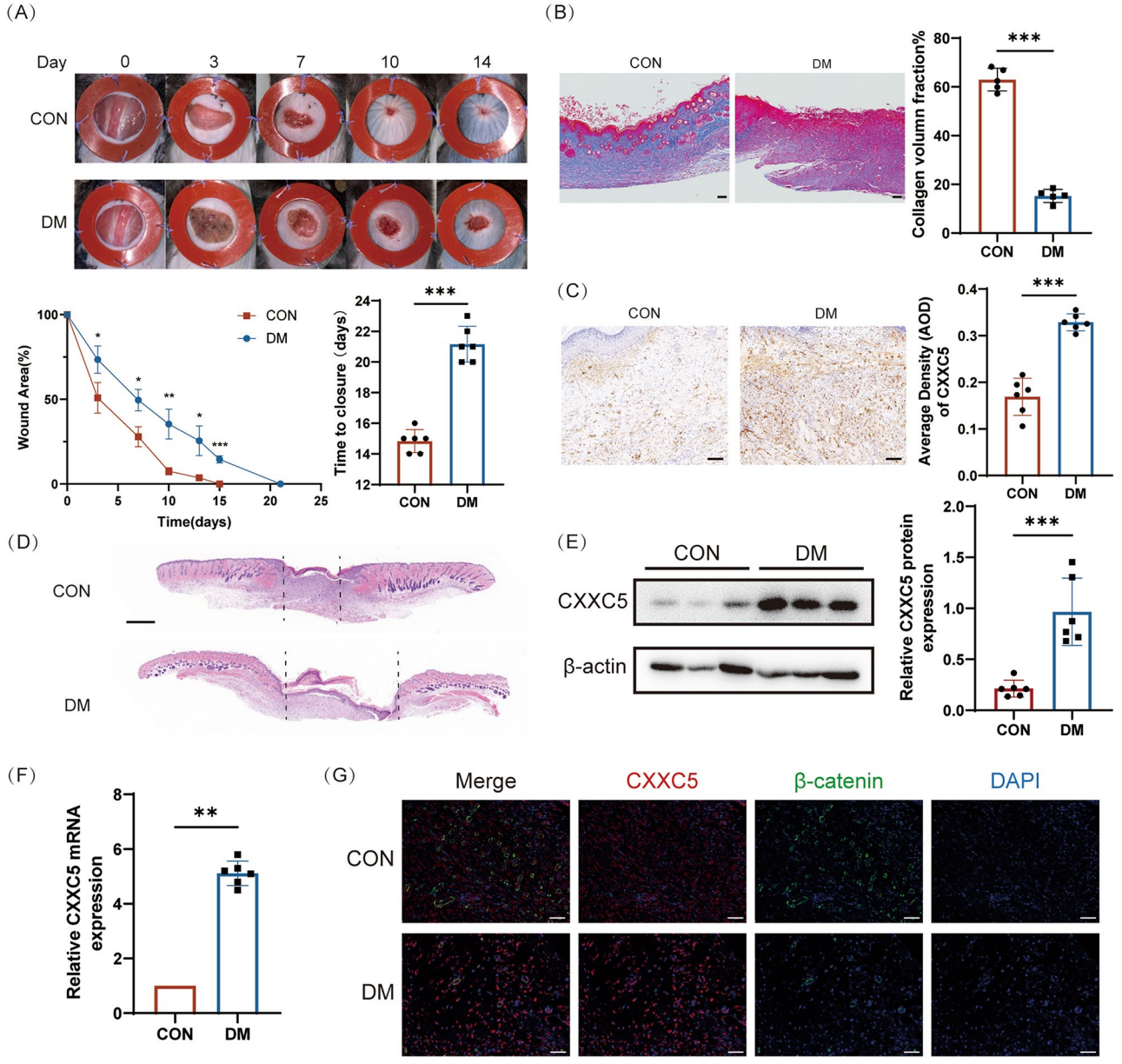

Fig. 1 Diabetic mice display chronically wound healing. **A** Schematic representation of changes and trends in postoperative wound healing. **B** MT staining of the CON ($n=5$) and DM ($n=5$). The quantity of collagen in the injured area on day 10. The scale bar is 100 μm. **C** IHC staining demonstrating levels of CXXC5 in wound tissue of CON and DM ($n=6$). The scale bar is 100 μm. **D** HE analysis of CON and DM, day 10 post-wounding. The scale bar is 1 mm. **E** WB data and **F** qRT-PCR test showing the expression of CXXC5 in skin tissues of CON and DM ($n=6$). **G** IF showed that β-catenin were reduced and CXXC5 was elevated in DM. ($n=6$). The scale bar is 50 μm. Data are displayed as mean ± SD. $^{*}P<0.05$, $^{**}P<0.01$, $^{***}P<0.001$

expression in the dermal wounds of DM relative to those of CON. Conversely, β-catenin and keratin 14 (Fig. S1A) expression patterns exhibited inverse correlations. Collectively, these results indicate that DM shows slower wound closure speed, less collagen deposition, and higher expression of CXXC5 in skin tissues than CON during wound healing.

KY19382 promotes wound closure in diabetic mice

In light of the up-regulation of CXXC5 in the peri-wound of diabetic mice, we postulated that blocking CXXC5 function might be essential in enhancing skin healing. KY19382 is a small molecule that can explicitly inhibit CXXC5-Dvl protein-protein interactions (PPIs) [28]. To investigate this further, we proceeded to apply KY19382 topically to back wounds in mice. Our results demonstrated that the wound repair of DM + KY19382 was better (Fig. 2A). Collagen deposition is essential

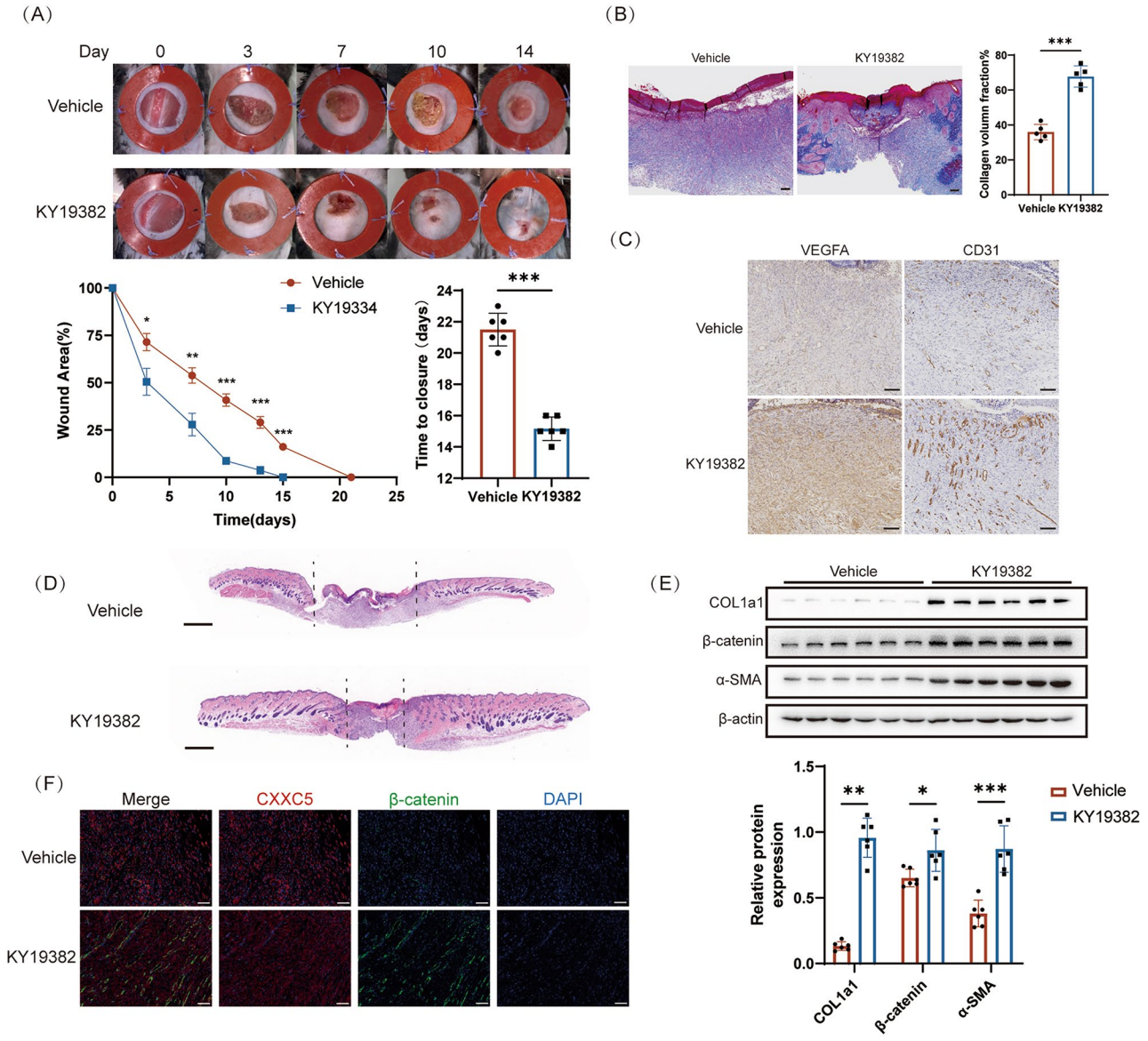

Fig. 2 KY19382 promotes wound closure in diabetic mice. **A** KY19382 decreased the skin wounds on the specified days. **B** MT staining of DM + Vehicle ($n = 5$) and DM + KY19382 ($n = 5$). Volume fraction of collagen within the injured area on day 10. The scale bar is 100 μm. **C** IHC tests demonstrating the levels of VEGFA and CD31 in skin tissues of DM + Vehicle and DM + KY19382 ($n = 5$). The scale bar is 100 μm. **D** HE examination of DM + Vehicle and DM + KY19382 on day 10 after injury ($n = 5$). The scale bar is 1 mm. **E** WB detected the expression of Col1a1, α-SMA, and β-catenin in the wound specimens of DM + Vehicle and DM + KY19382 ($n = 6$). **F** IF staining showed increased β-catenin levels in DM + KY19382 ($n = 6$). The scale bar is 50 μm. Data are displayed as mean ± SD.*$P < 0.05$, **$P < 0.01$, ***$P < 0.001$

for tissue repair and regeneration. MT staining analysis showed more collagen deposition in DM + KY19382 wounds compared with DM + Vehicle wounds (Fig. 2B). Then, we measured the levels of VEGFA and CD31 in the periwound tissues of mice using IHC staining. Similar to p-GSK3β (Fig. S2B), we found that both VEGFA and CD31 expression were higher in DG + KY19382 than in DM + vehicle (Fig. 2C). In addition, HE staining revealed that the distance between the edges of KY19382-treated wounds was shorter than in DM + Vehicle (Fig. 2D). Next, WB (Fig. 2E) and IF (Fig. 2F) were evaluated for collagen fiber synthesis and Wnt/β-catenin signaling pathway activation, revealing that the levels of myofibroblast markers (Col1a1, α-SMA), wound healing markers (keratin 14) (Fig S2A), and β-catenin in DM + KY19382 were elevated compared to DM + Vehicle. In conclusion, the results demonstrate that KY19382 accelerates the skin healing process by upregulating the Wnt/β-catenin signaling pathway, which benefits re-epithelialization, collagen deposition, and angiogenesis.

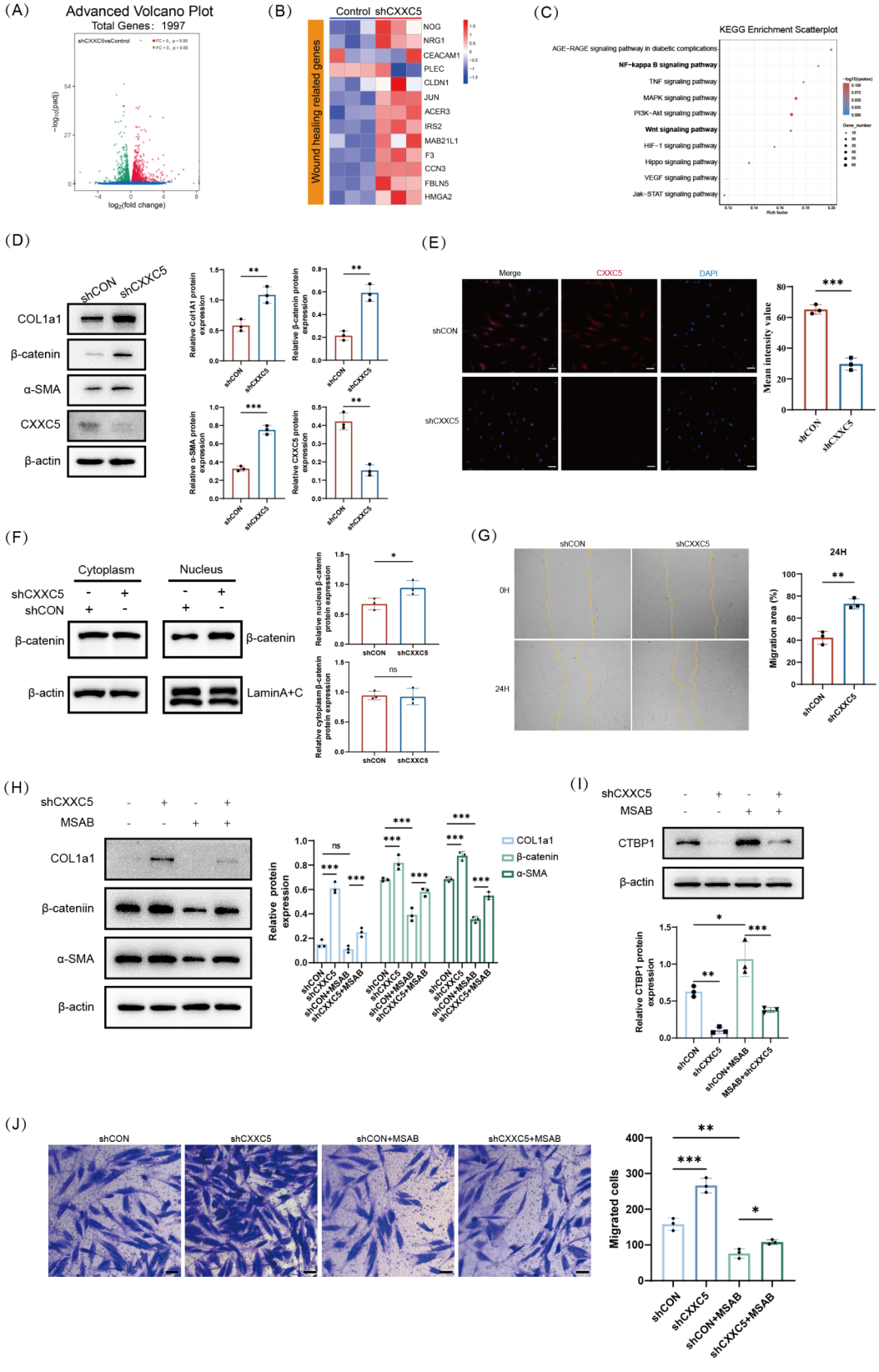

Fig. 3 (See legend on next page.)

(See figure on previous page.)

Fig. 3 Knockdown of CXXC5 enhances the growth and migration of HDFs through Wnt/β-catenin signaling pathway. **A** Differential expression of genes in shCXXC5 and shControl treated HDFs revealed by volcano plots ($n=3$). **B** Heatmap of differentially expressed genes associated with skin repair form RNA-Seq data based on|Log2FC|≥1.5 and $P<0.05$. **C** RNA-Seq data enrichment assessment by KEGG Pathway. **D** WB examined protein expression of β-catenin, Col1a1, α-SMA, and CXXC5 after the knockdown of CXXC5 in HDFs ($n=3$). **E** IF staining revealed the presence of HDFs in CON and shCXXC5 cells ($n=3$). Scale bar is 100 μm. **F** β-catenin levels in nuclear and cytoplasmic extracts were analyzed by WB. Lamin A + C and β-actin were performed as up-sampling controls for the nuclear and cytoplasmic sections ($n=3$). **G** Scratch wound tests were employed to assess the migratory capacity of HDFs in CON and shCXXC5 cells. **H** WB analysis of the influence of CXXC5 on the Wnt/β-catenin signaling pathway in HDFs ($n=3$). The quantitative analysis is shown in the bar chart. **I** WB was used to detect CTBP1 expression following administration of shCXXC5 and MSAB ($n=3$). **J** The migration capability of HDFs was analyzed using a Transwell analysis. ($n=3$). The results of the quantitative analysis are presented as a histogram. The scale bar is 100 μm. Data are displayed as mean ± SD. *$P<0.05$, **$P<0.01$, ***$P<0.001$

Knockdown of CXXC5 enhances the growth and migration of HDFs through Wnt/β-catenin signaling pathway

To uncover the molecular mechanism underlying the healing impact of CXXC5, we undertook RNA sequencing analysis of HDFs treated with shCXXC5 or shCON. Sequencing results showed that 1039 and 958 genes were markedly elevated and diminished, respectively (Fig. 3A). A heatmap demonstrated that the upregulation of genes was mainly associated with wound healing in response to shCXXC5 treatment (Fig. 3B). KEGG pathway enrichment analysis displayed that the increased genes were accumulated in many pathways, including the Wnt/β-catenin signaling pathway (Fig. 3C). We then examined the functional changes induced by the knockdown of CXXC5 in HDFs, as fibroblast migration and activation are critical for wound healing. Lentiviral transfection was used to knock down CXXC5 in HDFs, and puromycin was used to screen stably transfected cells (Fig. S3A, B). All the in vitro experiments were performed under high glucose, with hypertonicity as a control to prevent additional cell damage due to hypertonic effects, and the 40mM high glucose model was selected according to CCK8 data (Fig. S3C). WB showed that CXXC5 was effectively knocked down in HDFs, and the quantities of myofibroblast markers (CoL1a1 and α-SMA) were inversely elevated. β-catenin, a vital transcription regulator in Wnt/β-catenin signaling pathway, was also up-regulated (Fig. 3D). Cellular immunofluorescence confirmed attenuated CXXC5 fluorescence in HDFs of the shCXXC5-treated group (Fig. 3E). Stimulation of the Wnt/β-catenin signaling pathway results in suppression of β-catenin degradation through phosphorylation of downstream protein kinases, which in turn causes the subsequent stable aggregation of β-catenin entry into the nucleus, thereby initiating the transcription of downstream target genes. Therefore, we hypothesized that shCXXC5 may affect β-catenin nuclear translocation. Indeed, cytoplasmic and cytosolic isolation experiments showed that shCXXC5 triggered the nucleus aggregation of β-catenin (Fig. 3F). The scratch wound and transwell tests were then employed to detect the migration capacity of HDFs. Fused cells were scraped at the confluence of fibroblast monolayers to generate a migration space and were further cultured for 24 h. Knockdown of CXXC5 significantly promoted fibroblast migration at 24 h compared to the shCON (Fig. 3G), which was similar to the findings in the transwell migration analysis (Fig. S4A). The collective evidence indicates that the knockdown of CXXC5 promotes HDF migration and activation, which may be related to the Wnt/β-catenin signaling pathway.

To validate the involvement of the Wnt/β-catenin signaling pathway in the activation of HDFs induced by shCXXC5, we treated HDFs with MSAB. MSAB, a specific inhibitor of the Wnt/β-catenin signaling pathway, accelerates the degradation of β-catenin, thereby reducing Wnt/β-catenin downstream genes [34, 35]. HDFs were cultured with varying concentrations of MSAB (0, 0.6, 1.25, 2.5, 5, and 10 μM), and cell viability was recorded after 24, 48, and 72 h. The percentage of cell growth in the 2.5, 5 and 10 μM MSAB groups gradually decreased over time (Fig. S4B). Finally, 1.25 μM was chosen as the final concentration for cell treatment. MSAB effectively blocked shCXXC5-induced HDFs activation markers (Collagen I and α-SMA), eliminated the shCXXC5-induced promotion of β-catenin (Fig. 3H), and up-regulated C-terminal binding protein 1 (CtBP1) expression (Fig. 3I). CTBP1 is a co-repressor of transcription that directly inhibits the level of Wnt signaling pathway target genes [36, 37]. Moreover, MSAB significantly inhibited the migration and proliferation of shCXXC5-induced HDFs (Fig. 3J). These phenomena suggest that shCXXC5 directly induces the activation of HDFs via the Wnt/β-catenin signaling pathway.

shCXXC5-induced HDFs trigger the activation of HUVECs through NFκB and VEGFA/VEGFR2 signaling pathway

We also investigated the alterations induced by the knockdown of CXXC5 in HUVECs. We found that the neovascularization markers CD31 and p-NFκB were significantly reduced (Fig. 4A). This contrasts with the results of shCXXC5-induced HDFs. Further, the WB assay detected that the levels of VEGFA, VEGFR2, and p-IκBα were robustly increased in shCXXC5-induced HDFs (Fig. 4B, C). Therefore, we hypothesized that VEGFA, a cytokine highly secreted by HDFs, affects the physiological function of HUVECs in a paracrine manner.

We further elucidated the mechanism by which HUVECs are affected by shCXXC5-induced HDFs. The

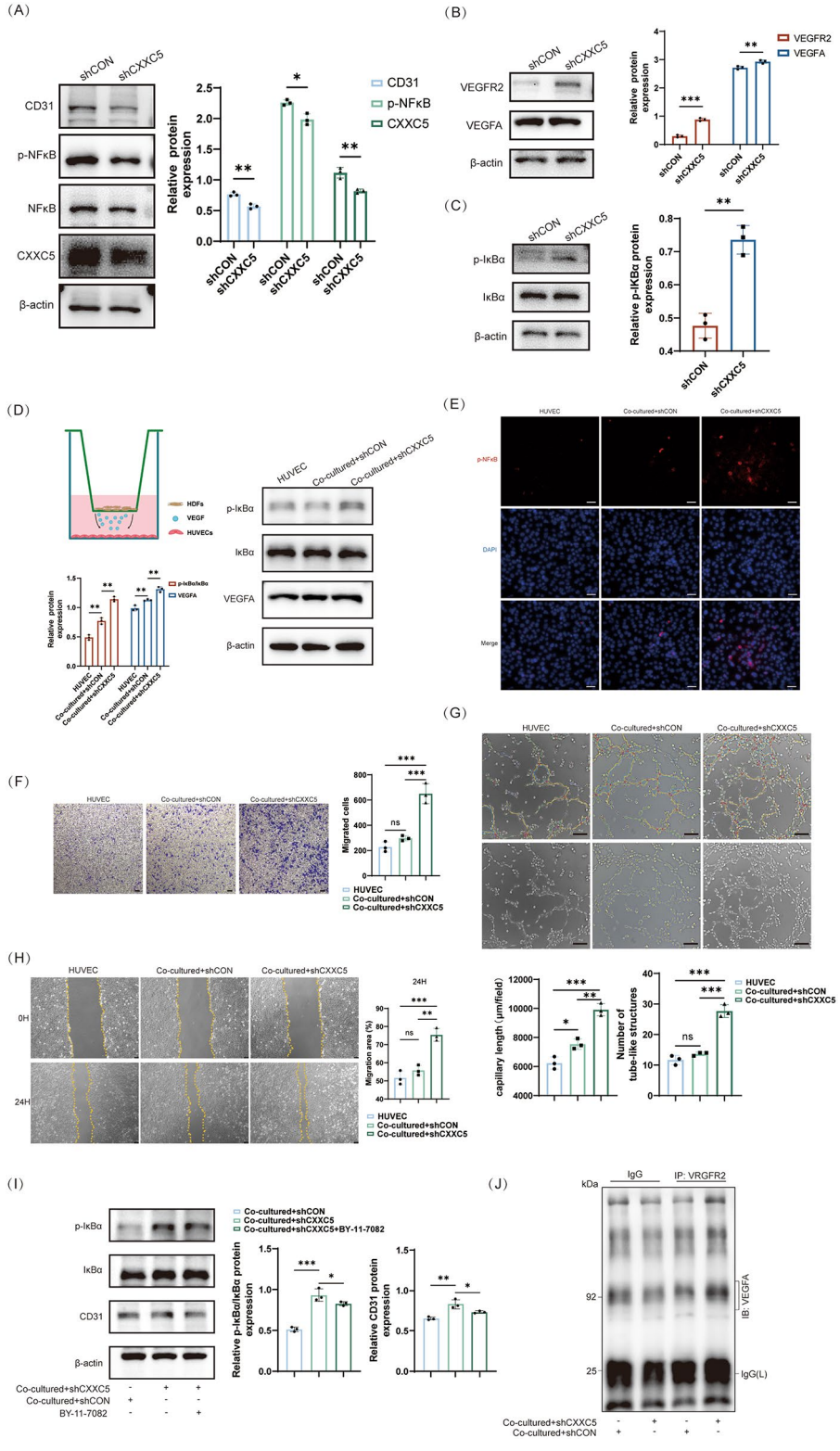

Fig. 4 (See legend on next page.)

(See figure on previous page.)

Fig. 4 shCXXC5-induced HDFs trigger the activation of HUVECs through VEGFA-VEGFR2 and NFκB signaling pathway. **A** The protein levels of CXXC5, CD31, p-NFκB, and NFκB were examined by WB after knocking down CXXC5 in HUVECs ($n=3$). **B** High levels of VEGFA and VEGFR2 were quantified by WB in HDFs after knockdown of CXXC5 ($n=3$). **C** WB was used to detect p-IκBα and IκBα expression in HDFs after the knockdown of CXXC5 ($n=3$). **D** Co-cultured of HDFs and HUVECs in chambers. Protein expression of p-IκBα, IκBα, and VEGFA was assessed by WB in the Co-culture systems ($n=3$). **E IF** showed that p-NFκB was nucleated in Co-cultured + shCXXC5 cells and was highly expressed compared to the other groups ($n=3$). **F**, **H** Transwell and Scratch wound tests were performed to analyze the migratory capacity of HUVECs ($n=3$). **G** Tube formation tests were utilized to assess the angiogenesis capacity of HUVECs ($n=3$). Quantitative analysis was performed using capillary length and number of tube sample structures. **I** WB was used to identify the extent of p-IκBα, IκBα, and CD31 in HUVECs after being treated with BAY-11-7082(5 μM) ($n=3$). **J** WB analysis was employed to assess the interactions between VEGFA and VEGFR2 ($n=3$) after IP with anti-VEGFA and anti-VEGFR2. The scale bar is 100 μm. Data are displayed as mean ± SD. $^{*}P<0.05$, $^{**}P<0.01$, $^{***}P<0.001$

protein expression of IκBα, p-IκBα, and VEGFA were tested by WB (Fig. 4D). These proteins above were markedly elevated in the Co-culture + shCXXC5 compared to the Co-cultured + shCON and the HUVEC-only. The IF results also revealed that p-NFκB entered the nucleus, and the fluorescence was significantly stronger in the Co-cultured + shCXXC5 (Fig. 4E). Modifications in signaling molecules during the process of wound repair have provided evidence that shCXXC5-induced HDFs are integral to the triggering of the NFκB signaling pathway. Furthermore, the combination of Co-cultured and shCXXC5 treatment was observed to significantly enhance cell migration in comparison to the Co-cultured + shCON. (Fig. 4F, H). In Co-cultured + shCXXC5, the number of tube-forming cells was higher. (Fig. 4G). To understand whether the angiogenic capacity of HUVECs promoted by Co-cultured + shCXXC5 treatment was related to the NFκB signaling pathway, we treated HUVECs with a NFκB-specific inhibitor (BAY-11-7082) and found that Co-cultured + shCXXC5 markedly increased the expression of CD31 and IκBα phosphorylation at S36, which was abrogated by BAY-11-7082 treatment (Fig. 4I). Meanwhile, IP analysis showed that Co-cultured + shCXXC5 treatment increased the binding of VEGFR2 and VEGFA in HUVECs (Fig. 4J). In summary, although the knockdown of CXXC5 in HUVECs may have a negative effect, cell-to-cell interactions should not be overlooked. Indeed, WB and IP experiments revealed that Co-cultured + shCXXC5 triggers the activation of HUVECs through the NFκB and VEGFA/VEGFR2 signaling pathway.

KY19382 promotes HUVECs migration and proliferation through hindering CTBP1 transcription to release NFκB

The above findings showed that the knockdown of CXXC5 had a negative effect on HUVECs. To clarify the molecular mechanism of CXXC5 in HUVECs, we used KY19382, an inhibitor that can specifically block the interaction between CXXC5 and Dvl. HUVECs were cultured with different concentrations of KY19382 (0, 0.01, 0.05, 0.1, and 0.2 mM), and cell viability was noted after 24, 48, and 72 h. The percentage of cell growth in the 0.1 and 0.2 mM KY19382 groups gradually decreased at 72 h (Fig. S5A). Finally, 0.1 mM was chosen as the final concentration for cell treatment. WB analysis showed that the levels of neovascular marker CD31, pro-angiogenesis factor VRGFA, VEGFR2, and cell proliferation biomarker PCNA were significantly elevated in HUVECs cultured with KY19382. Similarly, the phosphorylation levels of NFκB and IKKα were increased considerably (Fig. 5A). To elucidate whether the nuclear factor-κB (NFκB) signaling pathway actively regulates cellular proliferation and angiogenesis, KY19382-induced HUVECs were treated with BAY-11-7082. BAY-11-7082 effectively blocked KY19382-induced NFκB phosphorylation while eliminating KY19382-induced promotion of VEGFR2, CD31, and VEGFA expression (Fig. 5B). In addition, BAY-11-7082 significantly inhibited KY19382-promoted HUVECs migration (Fig. 5C, D, and S5B) and angiogenesis (Fig. 5E). In addition, we further found that CTBP1 expression was reduced in KY19382-induced HUVECs. An IP assay was conducted, followed by WB, in order to investigate the function of CTBP1 in KY19382-induced HUVECs. Our findings revealed that a notable proportion of CTBP1 was present in anti-IκBα complexes in KY19382-induced HUVECs, and these interactions were found to be reduced by BAY-11-7082 (Fig. 5F). A reduced proportion of CTBP1 was identified within anti-NFκB complexes in KY19382-induced HUVECs (Fig. 5G). Given that NFκB is binding to the inhibitory protein IκBα in an inactive state, we postulated that KY19382 might influence NFκB nuclear translocation through CTBP1. When considered collectively, these findings provide compelling evidence that KY19382 stimulates the migration, proliferation, and angiogenesis of HUVECs by activating the NFκB signaling pathway.

KY19382 induces HDFs activation through hinders CTBP1 transcription to stabilize β-catenin

Further research is underway to reveal the molecular mechanism behind the pro-healing function of KY19382 in HDFs. HDFs were cultured with different contents of KY19382 (0, 0.01, 0.05, 0.1, and 0.2 mM), and cell viability was revealed after 24, 48, and 72 h. The percentage of cell growth in the 0.1 and 0.2 mM KY19382 groups gradually decreased at 72 h (Fig. S6A). Finally, 0.1 mM was chosen as the final concentration for cell treatment. WB analysis showed that the levels of myofibroblast markers

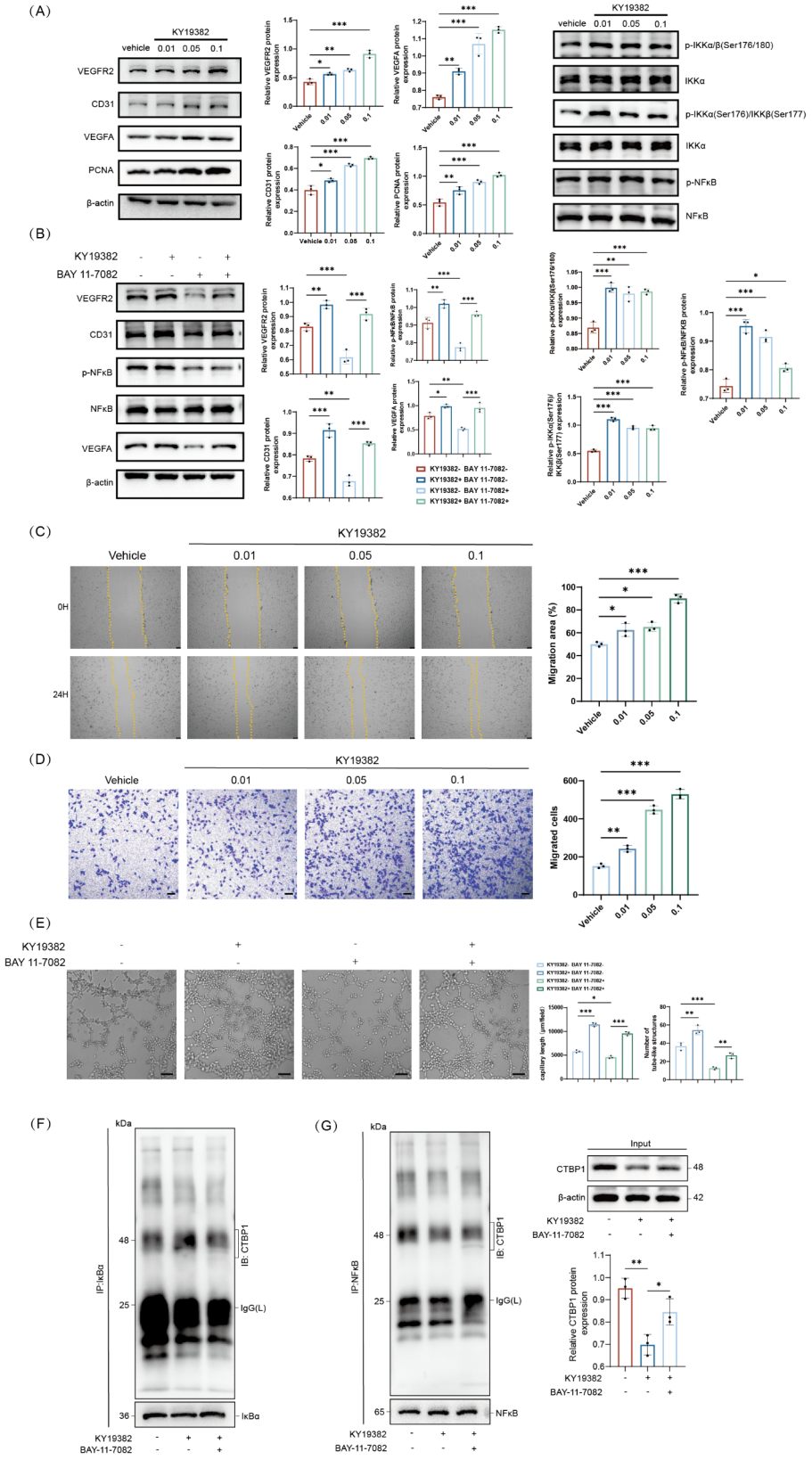

Fig. 5 (See legend on next page.)

(See figure on previous page.)

Fig. 5 KY19382 promotes HUVECs migration and proliferation through hindering CTBP1 transcription to release NFκB. **A** WB analysis of angiogenesis-related molecular biomarkers, PCNA, phosphorylated and NFκB associated proteins (IKKα and NFκB) at various KY19382 treatments in HUVECs ($n=3$). **B** HUVECs were co-cultured with the NFκB inhibitor BAY 11-7082 (5 μM) and KY19382 (0.1 mM) for 24 h. Expression of VEGFR2, CD31, p-NFκB, and VEGFA were assessed by WB ($n=3$). **C** Transwell and **D** Scratch wound tests were used to analyze the migration capacity of HUVECs ($n=3$). **E** Tube formation tests were employed to evaluate the angiogenic ability of HUVECs ($n=3$). **F** The interactions between IκBα and CTBP1 were evaluated by WB after IP with anti-IκBα and anti-CTBP1 ($n=3$). **G** WB ($n=3$) was applied to evaluate the interactions between NFκB and CTBP1. The scale bar is 100 μm. Data are displayed as mean ± SD.*$P<0.05$, **$P<0.01$, ***$P<0.001$

(Col1a1, α-SMA), β-catenin, Wnt signaling pathway transcription factors TCF1/TCF7, and the cell proliferation biomarker PCNA were significantly added in KY19382-treated HDFs (Fig. 6A), which could be eliminated MSAB (Fig. 6C). Subcellular isolation experiments showed that KY19382 triggered the nuclear localization of β-catenin, which was eliminated by Wnt/β-catenin inhibitors (Fig. 6B). Furthermore, MSAB significantly inhibited KY19382-promoted HDFs migration (Fig. 6D, E). An IP assay was next performed to determine whether CTBP1 was associated with β-catenin. We detected a fraction of β-catenin in the anti-TCF1/TCF7 complex in HDFs treated with shCXXC5 (Fig. S6B-C) and KY19382. Similarly, CTBP1 was recognized as a constituent of the anti-β-catenin complex, and the strength of these interactions was diminished by KY19382 (Fig. 6F). Since β-catenin is more stabilized in the nucleus, we postulated that the inhibition of CXXC5 might facilitate β-catenin nuclear translocation by reducing the interaction between the inhibitory factors CTBP1 and β-catenin. (Fig. 6G, and S6D).

Discussion

Diabetic skin repair represents a significant complication of diabetes, with a multitude of factors contributing to its pathogenesis, including four distinct stages of loss of compensation: inflammation, proliferation, angiogenesis, and remodeling [38]. Collagen deposition and angiogenesis provide a platform for cell migration and delivery of nutrients and cytokines during skin repair, which is vital for wound repair [9, 39].

Regenerative skin healing involves the transduction of multiple signaling pathways, of which the Wnt/β-catenin pathway is thought to play an critical role in tissue regrowth and skin fibrosis during wound healing [40]. Furthermore, both direct and indirect mediators of the NFκB signaling pathway, including VEGFA and VEGFR2, are essential for the regeneration of the vascular system [41]. Previous research has indicated that CXXC5 works not only as a negative regulator of the Wnt/β-catenin signaling pathway but also as a transcription driver required for HUVECs differentiation and vascular development [26]. Consequently, CXXC5 may represent an optimal target for the investigation of novel approaches to enhance diabetic wound repair.

In the present study, we demonstrated that β-catenin, an important mediator in the Wnt/β-catenin signaling pathway, was suppressed while CXXC5 expression was upregulated in streptozotocin-induced DM (Fig. 1C, E-G). Overexpression of CXXC5 has been proved to function as a negative regulator of the Wnt/β-catenin signaling pathway by interacting with Dvl in a series of disease models, including diabetic wound healing and baldness [16, 25, 29, 30]. This was similar to our findings, in which KY19382 treatment significantly improved wound healing rates in DM subjected to a 10 mm dorsal incision [28]. Progression of wound repair in DM with KY19382 was achieved by upregulation of skin regeneration markers (collagen I, α-SMA and keratin14), target genes essential for angiogenesis (CD31 and VRGFA) (Fig. 2C), and reversal of the inhibitory Wnt/β-catenin signaling pathway.

Our studies detected elevated VEGFA and VEGFR2 expression in shCXXC5-induced HDFs (Fig. 4B). Since VEGF is a cytokine released by fibroblasts that acts as a critical regulator of endothelial-mediated angiogenesis, we wondered whether intercellular paracrine effects were involved [14]. To further clarify the different cellular mechanisms underlying the effects of CXXC5 on HDFs and HUVECs, we conducted co-culture experiments of the two cell types. We found that Co-cultured + shCXXC5 indirectly triggered HUVECs migration and tube formation through activation of VEGFA/VEGFR2 and NAKB signaling pathways (Fig. 4I, J). Previous works have illustrated that the NFκB pathway serves as a pivotal regulator of several physiological processes, including inflammatory reaction, immune response, cell growth, and death [42, 43]. However, genes for proteins that mediate neoangiogenesis are induced by NFκB, including VEGF (the main component of the vasculogenic family), and sustained elevation of NFκB increases the transcription of the VEGF gene [18, 22]. Wang et al. [24] found that B7-H3 increased the expression of VEGFA and angiogenesis in an NFκB pathway-dependent manner. In another study, SLURP1 was shown to prevent the formation of HUVEC tubes by inhibiting the nuclear localization of NFκB [44]. This reveals that increased NFκB activity may promote the proliferation and vascularization of HUVECs. Interestingly, the same knockdown of CXXC5 in HUVECs in our study resulted in the unexpected inhibition of the neovascularization marker CD31 and the NFκB signaling pathway. This is due to the fact that CXXC5 is a transcriptional activator of Flk-1 that promotes differentiation and migration of endothelial cells

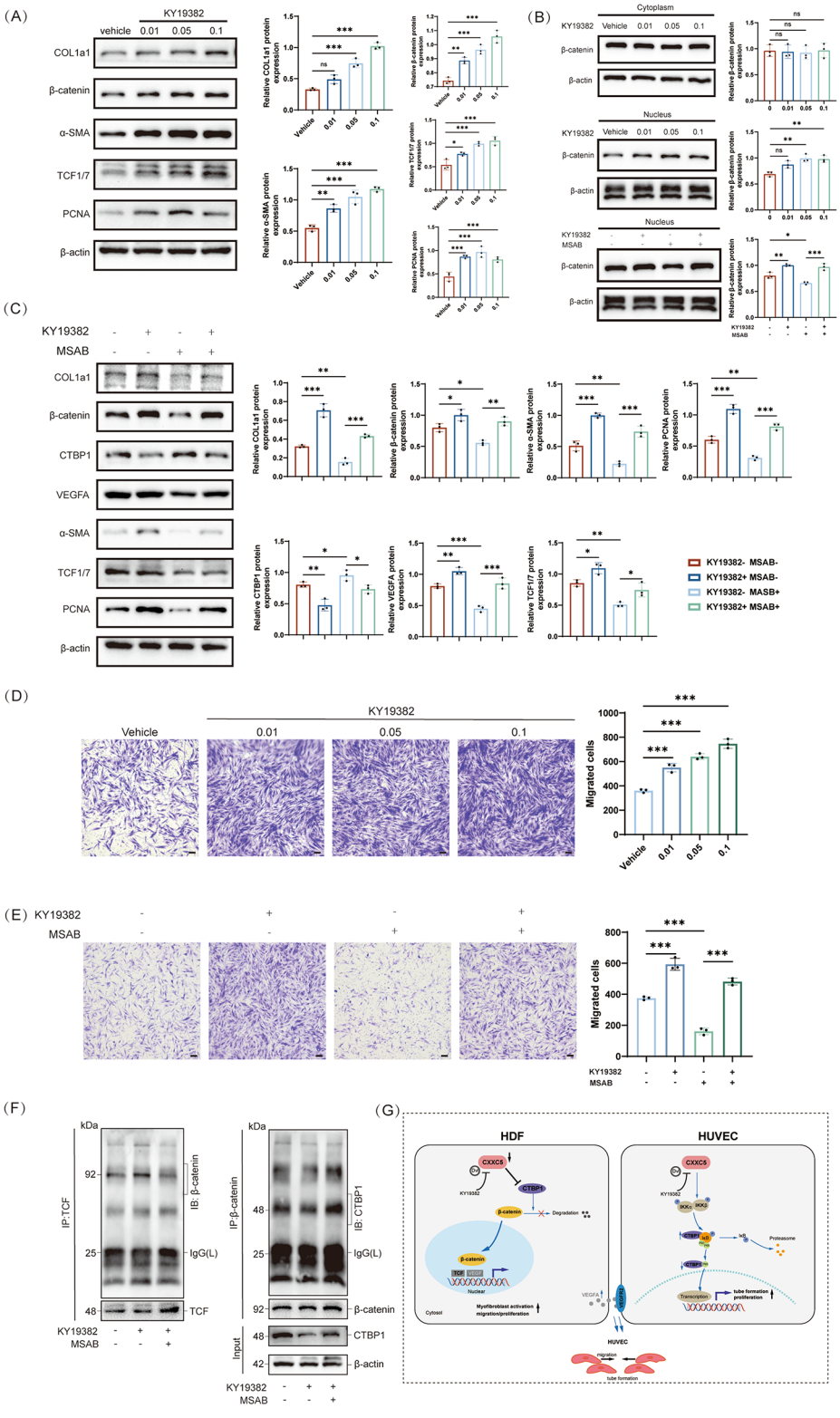

Fig. 6 (See legend on next page.)

(See figure on previous page.)

Fig. 6 KY19382 induces HDFs activation through hinders CTBP1 transcription to stabilize β-catenin. **A** WB analysis of HDFs activation-related molecular markers, β-catenin, and downstream targets of the Wnt signaling pathway ($n=3$). **B** Nuclear and cytoplasmic β-catenin levels were quantified by WB. The nuclear and cytoplasmic fractions were validated using Lamin A + C and β-actin as controls ($n=3$). **C** HDFs were Co-cultured with the Wnt/β-catenin inhibitor MSAB (1.25 μM) and KY19382 (0.1 mM) within 24 h. Lysates were evaluated by WB using the indicated antibodies ($n=3$). **D**, **E** Transwell assay measuring cell migration capability following a 48-hour treatment period ($n=3$). **F** HDFs were exposed to KY19382 (0.1mM) or MSAB (1.25μM) in 24 h. Anti-TCF1 /TCF7 and anti-β-catenin antibodies were used to immunoprecipitated the lysates. Western blotting ($n=3$) was performed to evaluate the association between TCF1/TCF7, β-catenin, and CTBP1. **G** Schematic illustrating the molecular function of CXXC5 in speeding up diabetic skin repair. The scale bar is 100 μm. Data are displayed as mean ± SD. $^{*}P<0.05$, $^{**}P<0.01$, $^{***}P<0.001$

and angiogenesis [26]. Similarly, earlier studies [16]failed to find improved healing in diabetes-induced CXXC5 knockout mice. Based on these discoveries, we speculated that the beneficial effects of fibroblasts on endothelial cells after knockdown of CXXC5 in vitro system could not compensate for the negative impact of failure to encode the downstream angiogenic factor VEGFR2 after the absence of the transcriptional activator CXXC5 in Flk-1 [26]. Therefore, instead of directly knocking down CXXC5, we further administered KY19382 in HUVECs to block the function of CXXC5 and found that both angiogenesis-related genes and the NFκB signaling pathway were activated. These unexpected results suggest that specific elimination of CXXC5 interaction with Dvl, rather than direct knockdown, has a beneficial effect on HUVECs and that the impact of CXXC5 on wound remodeling may differ between cell types. Therefore, to uncover the mechanisms involved, it is required to explore the interplay between vascular endothelial cells and fibroblasts in the action of CXXC5 on skin regeneration [45].

CTBP1 is a transcriptional co-repressor with two isoforms (CTBP1, CTBP2) involved in gene expression, cell cycle progression, and regulation of cell proliferation, apoptosis, and survival [46–48]. CTBP binding DNA indirectly to several DNA-binding chaperones, including E-calmodulin repression in epithelial cells and breast cancer susceptibility protein type 1 (BRCA1) transcription in cancer cells [48, 49]. Huard et al. [50] provided evidence that CTBP1 interacts with DNA-binding transcription elements in the nucleus, including the Wnt/β-catenin/T cytokine (TCF) complex, promotes transcriptional repression by recruiting chromatin-modifying enzymes, and proposed that CtBP1 is a repressor of Wnt signaling. Furthermore, our study reported that application of KY19382 in HUVECs enhanced the interaction of CTBP1 with IκBα (Fig. 5F) and suppressed the binding of IκBα to NFκB, followed by the dissociation of NFκB from the trimeric complex (Fig. 5G) and the activation of the NFκB signaling pathway, which in return promotes the transcription of the downstream related gene VEGF. As confirmed by immunoprecipitation of CTBP1 and β-catenin after administration of shCXXC5 and KY19382 in HDFs (Fig. 6F), blockade of CXXC5 signaling in HDFs reduced the binding of CTBP1 to β-catenin and enhanced the nuclear enrichment and stabilization of β-catenin (Fig S6D), thereby promoting the transcription of the TCF/LEF family (Fig S6B, C). Accordingly, we speculated that the negative regulation of the wnt/β-catenin and NFκB signaling pathways by CXXC5 function in diabetic wound healing may be related to the regulation of the transcriptional co-repressor CTBP1.

In summary, restoration of the inhibited Wnt/β-catenin signaling pathway by KY19382, which specifically hinders CXXC5-Dvl interaction, appears to be a potential therapeutic strategy for diabetic skin repair. However, our study only focused on the molecular mechanisms of HDFs and HUVECs under high glucose. Kim et al. [16] suggested that CXXC5 functions differently in diabetic and normal mice, and we would investigate this in the next experiments. Another future direction of our research is to consider the effects of CXXC5 on other phases of skin healing, such as inflammation. In addition, we will be working to develop a new platform for the practical integration of specific small interferons with biomedical materials for clinical, which makes great sense.

Conclusion

In conclusion, our studies in mice and cellular models of wound healing suggest that CXXC5 function blockade activates the Wnt/β-catenin, VEGFA/VEGFR2, and NFκB signaling pathways within skin regeneration, inducing fibroblast to myofibroblast transdifferentiation and HUVEC migration and tube formation, respectively, thereby benefiting chronic wound healing in diabetes. Our findings present new evidence for the previously unnoticed specific mechanistic role of CXXC5 in chronic diabetic skin repair.

Supplementary Information

The online version contains supplementary material available at https://doi.org/10.1186/s12964-025-02097-z.

Supplementary Material 1

Acknowledgements
Not applicable.

Author contributions
Q.T. was responsible for the initial design and experimental strategy of this research. Y.C. and X.D. established the diabetic mouse wound model and conducted the experiments. S.S., Y.H., and X.S. participated in data collection.

H.H., B.W., H.Z., and Z.M. contributed to the data analysis and drafted the manuscript.

Funding
This work was funded by the National Natural Science Foundation of China (81671922, 81974288).

Data availability
All data during this work are provided by the corresponding author upon suitable request. rRNA sequencing FASTQ files relevant to this article is available on [https://www.ncbi.nlm.nih.gov/sra/PRJNA1114900], hosted at the National Centre for Biotechnology Information Sequence Read Archive (SRA) database (PRJNA1114900).

Declarations

Ethics approval and consent to participate
The proposed animal experiment has been authorized by the Medical School for Animal Use and Care Committee of Nanjing Drum Tower (Ethics Approval Number: DWSY-22083209) in adherence to ARRIVE guidelines.

Consent for publication
All the authors give their consent for publication.

Competing interests
The authors declare no competing interests.

Author details
[1]Department of Burns and Plastic Surgery, Affiliated Hospital of Medical School, Nanjing Drum Tower Hospital, Nanjing University, Nanjing, China
[2]Department of Dermatologic Surgery, Shanghai Skin Disease Hospital, Tongji University School of Medicine, Shanghai, China
[3]Department of Burn and Plastic Surgery, Gulou Clinical Medical College of Nanjing Medical University, Nanjing, China
[4]Department of Plastic and Aesthetic Surgery, The Second Affiliated Hospital of Soochow University, Suzhou, China
[5]Department of Burns and Plastic Surgery, Nanjing Drum Tower Hospital Clinical College of Traditional Chinese and Western Medicine, Nanjing University of Chinese Medicine, Nanjing, China
[6]Department of Burns and Plastic Surgery, Nanjing Drum Tower Hospital Clinical College of Jiangsu University, Nanjing, China
[7]Department of Burns and Plastic Surgery, Nanjing Drum Tower Hospital Clinical College of Nanjing University of Chinese Medicine, Nanjing, China
[8]Department of Burns and Plastic Surgery, Anqing Shihua Hospital, Nanjing Drum Tower Hospital Group, Anqing, China

Received: 23 October 2024 / Accepted: 9 February 2025
Published online: 25 February 2025

References

1. Zheng Y, Ley SH, Hu FB. Global aetiology and epidemiology of type 2 diabetes mellitus and its complications. Nat Rev Endocrinol. 2018;14:88–98.
2. Tian WQ, Chen SY, Chuan FN, Zhao WR, Zhou B. Down-regulated TINAGL1 in fibroblasts impairs wound healing in diabetes. Faseb j. 2022;36:e22235.
3. Volmer-Thole M, Lobmann R. Neuropathy and Diabetic Foot Syndrome. Int J Mol Sci 2016, 17.
4. Wang F, Zhang X, Zhang J, Xu Q, Yu X, Xu A, Yi C, Bian X, Shao S. Recent advances in the adjunctive management of diabetic foot ulcer: focus on noninvasive technologies. Med Res Rev. 2024;44:1501–44.
5. Senneville É, Albalawi Z, van Asten SA, Abbas ZG, Allison G, Aragón-Sánchez J, Embil JM, Lavery LA, Alhasan M, Oz O, et al. Diagnosis of infection in the foot of patients with diabetes: a systematic review. Diabetes Metab Res Rev. 2024;40:e3723.
6. Lipsky BA, Berendt AR, Cornia PB, Pile JC, Peters EJ, Armstrong DG, Deery HG, Embil JM, Joseph WS, Karchmer AW, et al. 2012 Infectious Diseases Society of America clinical practice guideline for the diagnosis and treatment of diabetic foot infections. Clin Infect Dis. 2012;54:e132–173.
7. Jones A, Hinchliffe R. Acute diabetic foot disease. Br J Surg 2024, 111.
8. Bi H, Li H, Zhang C, Mao Y, Nie F, Xing Y, Sha W, Wang X, Irwin DM, Tan H. Stromal vascular fraction promotes migration of fibroblasts and angiogenesis through regulation of extracellular matrix in the skin wound healing process. Stem Cell Res Ther. 2019;10:302.
9. Chang M, Nguyen TT. Strategy for Treatment of Infected Diabetic Foot Ulcers. Acc Chem Res. 2021;54:1080–93.
10. Martin P, Nunan R. Cellular and molecular mechanisms of repair in acute and chronic wound healing. Br J Dermatol. 2015;173:370–8.
11. Veith AP, Henderson K, Spencer A, Sligar AD, Baker AB. Therapeutic strategies for enhancing angiogenesis in wound healing. Adv Drug Deliv Rev. 2019;146:97–125.
12. Liu Y, Liu Y, He W, Mu X, Wu X, Deng J, Nie X. Fibroblasts: immunomodulatory factors in refractory diabetic wound healing. Front Immunol. 2022;13:918223.
13. Nakatsu MN, Sainson RC, Aoto JN, Taylor KL, Aitkenhead M, Pérez-del-Pulgar S, Carpenter PM, Hughes CC. Angiogenic sprouting and capillary lumen formation modeled by human umbilical vein endothelial cells (HUVEC) in fibrin gels: the role of fibroblasts and Angiopoietin-1. Microvasc Res. 2003;66:102–12.
14. Fukumura D, Xavier R, Sugiura T, Chen Y, Park EC, Lu N, Selig M, Nielsen G, Taksir T, Jain RK, Seed B. Tumor induction of VEGF promoter activity in stromal cells. Cell. 1998;94:715–25.
15. Claesson-Welsh L, Welsh M. VEGFA and tumour angiogenesis. J Intern Med. 2013;273:114–27.
16. Kim E, Seo SH, Hwang Y, Ryu YC, Kim H, Lee KM, Lee JW, Park KH, Choi KY. Inhibiting the cytosolic function of CXXC5 accelerates diabetic wound healing by enhancing angiogenesis and skin repair. Exp Mol Med. 2023;55:1770–82.
17. Lee SH, Kim MY, Kim HY, Lee YM, Kim H, Nam KA, Roh MR, Min do S, Chung KY, Choi KY. The dishevelled-binding protein CXXC5 negatively regulates cutaneous wound healing. J Exp Med. 2015;212:1061–80.
18. Bakshi HA, Quinn GA, Nasef MM, Mishra V, Aljabali AAA, El-Tanani M, Serrano-Aroca Á, Webba Da Silva M, McCarron PA, Tambuwala MM. Crocin Inhibits Angiogenesis and Metastasis in Colon Cancer via TNF-α/NF-κB/VEGF Pathways. Cells 2022, 11.
19. Xie J, Zhang H, Wang K, Ni J, Ma X, Khoury CJ, Prifti V, Hoard B, Cerenzia EG, Yin L, et al. M6A-mediated-upregulation of lncRNA BLACAT3 promotes bladder cancer angiogenesis and hematogenous metastasis through YBX3 nuclear shuttling and enhancing NCF2 transcription. Oncogene. 2023;42:2956–70.
20. Zhang C, Wu D, Dong B, Liao G, Yu Y, Huang S, Luo F, Zhang B, Wu H, Li T, et al. The scaffold of neutrophil extracellular traps promotes CCA progression and modulates angiogenesis via ITGAV/NFκB. Cell Commun Signal. 2024;22:103.
21. Zhao X, Li L, Yuan S, Zhang Q, Jiang X, Luo T. SPIB acts as a tumor suppressor by activating the NFκB and JNK signaling pathways through MAP4K1 in colorectal cancer cells. Cell Signal. 2021;88:110148.
22. Xie TX, Xia Z, Zhang N, Gong W, Huang S. Constitutive NF-kappaB activity regulates the expression of VEGF and IL-8 and tumor angiogenesis of human glioblastoma. Oncol Rep. 2010;23:725–32.
23. Dudics S, Langan D, Meka RR, Venkatesha SH, Berman BM, Che CT, Moudgil KD. Natural products for the treatment of Autoimmune Arthritis: their mechanisms of action, targeted delivery, and interplay with the host Microbiome. Int J Mol Sci 2018, 19.
24. Wang R, Ma Y, Zhan S, Zhang G, Cao L, Zhang X, Shi T, Chen W. B7-H3 promotes colorectal cancer angiogenesis through activating the NF-κB pathway to induce VEGFA expression. Cell Death Dis. 2020;11:55.
25. Kim HY, Yoon JY, Yun JH, Cho KW, Lee SH, Rhee YM, Jung HS, Lim HJ, Lee H, Choi J, et al. CXXC5 is a negative-feedback regulator of the Wnt/β-catenin pathway involved in osteoblast differentiation. Cell Death Differ. 2015;22:912–20.
26. Kim HY, Yang DH, Shin SW, Kim MY, Yoon JH, Kim S, Park HC, Kang DW, Min D, Hur MW, Choi KY. CXXC5 is a transcriptional activator of Flk-1 and mediates bone morphogenic protein-induced endothelial cell differentiation and vessel formation. Faseb j. 2014;28:615–26.
27. Seo SH, Kim E, Yoon M, Lee SH, Park BH, Choi KY. Metabolic improvement and liver regeneration by inhibiting CXXC5 function for non-alcoholic steatohepatitis treatment. Exp Mol Med. 2022;54:1511–23.
28. Ryu YC, Lee DH, Shim J, Park J, Kim YR, Choi S, Bak SS, Sung YK, Lee SH, Choi KY. KY19382, a novel activator of Wnt/β-catenin signalling, promotes hair regrowth and hair follicle neogenesis. Br J Pharmacol. 2021;178:2533–46.
29. Choi S, Kim HY, Cha PH, Seo SH, Lee C, Choi Y, Shin W, Heo Y, Han G, Lee W, Choi KY. CXXC5 mediates growth plate senescence and is a target for enhancement of longitudinal bone growth. Life Sci Alliance 2019, 2.

30. Lee SH, Seo SH, Lee DH, Pi LQ, Lee WS, Choi KY. Targeting of CXXC5 by a competing peptide stimulates Hair Regrowth and Wound-Induced Hair Neogenesis. J Invest Dermatol. 2017;137:2260–9.
31. Seo SH, Kim E, Lee SH, Lee YH, Han DH, Go H, Seong JK, Choi KY. Inhibition of CXXC5 function reverses obesity-related metabolic diseases. Clin Transl Med. 2022;12:e742.
32. Yoon M, Kim E, Seo SH, Kim GU, Choi KY. KY19382 accelerates cutaneous Wound Healing via activation of the Wnt/β-Catenin signaling pathway. Int J Mol Sci 2023, 24.
33. Seo SH, Kim E, Joo Y, Lee J, Oh KT, Hwang SJ, Choi KY. A mixed Micellar Formulation for the Transdermal Delivery of an Indirubin Analog. Pharmaceutics 2020, 12.
34. Hwang SY, Deng X, Byun S, Lee C, Lee SJ, Suh H, Zhang J, Kang Q, Zhang T, Westover KD, et al. Direct targeting of β-Catenin by a small molecule stimulates proteasomal degradation and suppresses oncogenic Wnt/β-Catenin signaling. Cell Rep. 2016;16:28–36.
35. Liu H, Liu Y, Zhou Y, Chen X, Pan S, Zhou Q, Ji H, Zhu X. TM7SF2-induced lipid reprogramming promotes cell proliferation and migration via CPT1A/Wnt/β-Catenin axis in cervical cancer cells. Cell Death Discov. 2024;10:207.
36. Valenta T, Lukas J, Korinek V. HMG box transcription factor TCF-4's interaction with CtBP1 controls the expression of the wnt target Axin2/Conductin in human embryonic kidney cells. Nucleic Acids Res. 2003;31:2369–80.
37. Shooshtarizadeh P, Helness A, Vadnais C, Brouwer N, Beauchemin H, Chen R, Bagci H, Staal FJT, Coté JF, Möröy T. Gfi1b regulates the level of Wnt/β-catenin signaling in hematopoietic stem cells and megakaryocytes. Nat Commun. 2019;10:1270.
38. Louiselle AE, Niemiec SM, Zgheib C, Liechty KW. Macrophage polarization and diabetic wound healing. Transl Res. 2021;236:109–16.
39. Zhang H, Nie X, Shi X, Zhao J, Chen Y, Yao Q, Sun C, Yang J. Regulatory mechanisms of the Wnt/β-Catenin pathway in Diabetic Cutaneous Ulcers. Front Pharmacol. 2018;9:1114.
40. Jere SW, Houreld NN. Regulatory processes of the Canonical Wnt/β-Catenin pathway and Photobiomodulation in Diabetic Wound Repair. Int J Mol Sci 2022, 23.
41. Huang X, Liang P, Jiang B, Zhang P, Yu W, Duan M, Guo L, Cui X, Huang M, Huang X. Hyperbaric oxygen potentiates diabetic wound healing by promoting fibroblast cell proliferation and endothelial cell angiogenesis. Life Sci. 2020;259:118246.
42. Barnabei L, Laplantine E, Mbongo W, Rieux-Laucat F, Weil R. NF-κB: at the Borders of autoimmunity and inflammation. Front Immunol. 2021;12:716469.
43. White S, Lin L, Hu K. NF-κB and tPA signaling in kidney and other diseases. Cells 2020, 9.
44. Swamynathan S, Loughner CL, Swamynathan SK. Inhibition of HUVEC tube formation via suppression of NFκB suggests an anti-angiogenic role for SLURP1 in the transparent cornea. Exp Eye Res. 2017;164:118–28.
45. Newman AC, Nakatsu MN, Chou W, Gershon PD, Hughes CC. The requirement for fibroblasts in angiogenesis: fibroblast-derived matrix proteins are essential for endothelial cell lumen formation. Mol Biol Cell. 2011;22:3791–800.
46. Chan KL, Gomez J, Cardinez C, Kumari N, Sparbier CE, Lam EYN, Yeung MM, Garciaz S, Kuzich JA, Ong DM, et al. Inhibition of the CtBP complex and FBXO11 enhances MHC class II expression and anti-cancer immune responses. Cancer Cell. 2022;40:1190–e12061199.
47. Birts CN, Bergman LM, Blaydes JP. CtBPs promote mitotic fidelity through their activities in the cell nucleus. Oncogene. 2011;30:1272–80.
48. Grooteclaes M, Deveraux Q, Hildebrand J, Zhang Q, Goodman RH, Frisch SM. C-terminal-binding protein corepresses epithelial and proapoptotic gene expression programs. Proc Natl Acad Sci U S A. 2003;100:4568–73.
49. Deng H, Li F, Li H, Deng Y, Liu J, Wang D, Han G, Wang XJ, Zhang Q. CtBP1 overexpression in keratinocytes perturbs skin homeostasis. J Invest Dermatol. 2014;134:1323–31.
50. Huard CC, Tremblay CS, Helsper K, Delisle MC, Schindler D, Lévesque G, Carreau M. Fanconi anemia proteins interact with CtBP1 and modulate the expression of the wnt antagonist Dickkopf-1. Blood. 2013;121:1729–39.

Publisher's note